ENVIRONMENTAL RESEARCH
CLIMATE

North American cooling signature of strong stratospheric wave events depends on the QBO phase

ENVIRONMENTAL RESEARCH
CLIMATE

CrossMark

OPEN ACCESS

RECEIVED
12 March 2024

REVISED
20 May 2024

ACCEPTED FOR PUBLICATION
4 June 2024

PUBLISHED
18 June 2024

LETTER

North American cooling signature of strong stratospheric wave events depends on the QBO phase

Xiuyuan Ding[1,*], **Gang Chen**[1,*] **and Gudrun Magnusdottir**[2]

[1] Department of Atmospheric and Oceanic Sciences, University of California, Los Angeles, CA, United States of America
[2] Department of Earth System Science, University of California, Irvine, CA, United States of America
[*] Authors to whom any correspondence should be addressed.

E-mail: dingxy@ucla.edu and gchenpu@ucla.edu

Keywords: stratosphere-troposphere coupling, cold extremes, QBO

Supplementary material for this article is available online

Abstract

Extreme stratospheric wave activity has been linked to surface cold extremes over North America, but little is known whether the Quasi-biennial Oscillation (QBO) plays a role in this linkage. Here, by comparing strong stratospheric wave events during the westerly phase (wQBO) with those during the easterly phase (eQBO), we show that the cooling signature following strong wave events depends on the QBO phase in observations. During wQBO, strong wave events are followed by an increased risk of North American cold extremes and a vertical structure shift from a westward phase tilt to an eastward tilt. However, strong wave events under eQBO do not change the cold risk nor alter the vertical tilt. We further examine this dependence on QBO in QBO-resolving climate models, finding that the cooling signature of strong wave events in models is largely insensitive to QBO phases. This insensitivity is suggested to be linked to model biases in the stratospheric wave representation.

1. Introduction

Anthropogenic global warming is anticipated to reduce wintertime cold extremes (Lorenz *et al* 2019, Oldenborgh *et al* 2019), yet recent years have witnessed extreme cold events driven by atmospheric dynamics (Johnson *et al* 2018, Ma and Zhu 2019, Cohen *et al* 2021, 2023). These observations have heated the ongoing debate on the drivers of cold spells (Hartmann 2015, Harnik *et al* 2016, Zhang *et al* 2018, 2022, Blackport *et al* 2019, Albers *et al* 2022). Of particular interest is the role of the stratosphere (Kolstad *et al* 2010, Yu *et al* 2015, Cohen *et al* 2021, Huang *et al* 2021, Davis *et al* 2022). There is increasing evidence that extreme stratospheric wave variability contributes to surface cold waves through planetary wave reflection (Shaw and Perlwitz 2013, Kretschmer *et al* 2018, Cohen *et al* 2021, Liang *et al* 2022, Messori *et al* 2022, Millin *et al* 2022, Reichler and Jucker 2022, Shen *et al* 2022, Zou *et al* 2023, Zou and Zhang 2024). Using observations and climate models, Ding *et al* (2023b) demonstrate that strong stratospheric wave activity is followed by changes in the vertical coupling of planetary waves, with an increased risk of cold extremes over North America.

Considering the dominant role of the Quasi-biennial Oscillation (QBO) in the tropical stratosphere, it becomes pertinent to investigate whether the QBO modulates the coupling of stratospheric wave variability with the surface. The QBO has been extensively studied for its influence on the stratospheric polar vortex and associated teleconnections (Baldwin *et al* 2001, Labe *et al* 2019, Rao *et al* 2020, Anstey *et al* 2022a). With roughly 28 month periodic variations in equatorial stratospheric zonal wind, the QBO's high predictability holds great implications for surface predictions (Thompson *et al* 2002, Pohlmann *et al* 2013, Scaife *et al* 2014, Stockdale *et al* 2022, Anstey *et al* 2022a). As first hypothesized by Holton and Tan (1980), the QBO can affect the strength of the stratospheric polar vortex by altering planetary wave propagation. In general, the polar vortex weakens when the QBO is in its easterly phase (e.g. Andrews *et al* 2019, Zhang *et al* 2019, Elsbury *et al* 2021b). A weakened polar vortex often leads to the downward propagation of the negative

Northern Annular Mode (NAM) and persistent mid-latitude cold anomalies at the surface (Baldwin and Dunkerton 2001, Sigmond *et al* 2013, Domeisen *et al* 2020, Baldwin *et al* 2021).

However, to our knowledge, the role of the QBO phase in the surface signature of strong stratospheric wave activity or wave reflection events remains unexplored. Ding *et al* (2023a) emphasize the crucial role of the planetary wave pattern in the stratosphere-troposphere coupling during strong wave events, suggesting that altering the planetary wave propagating environment could affect these events and their surface linkages. Messori *et al* (2022) notice that wave reflection events preferentially occur during the westerly phase of the QBO in observations. Sensitivity experiments with CESM1 indicate that the surface signal of downward wave reflection is stronger in the absence of the QBO (Lubis *et al* 2016).

In this paper, we subsample strong stratospheric wave events according to QBO phases and show that strong wave events during the westerly QBO (wQBO) increase the risk of North American (NA) cold extremes while those during the easterly QBO (eQBO) do not. This suggests that the QBO may provide predictability for cold air outbreaks on sub-seasonal timescales by modulating the coupling of strong wave events. However, we find that climate models struggle to replicate this dependence on QBO phases. We further attribute the discrepancy between models and reanalysis to the different evolutions of stratospheric circulation following strong stratospheric wave events.

2. Data and methods

2.1. Reanalysis and climate models

We analyze the daily data from the fifth generation of atmospheric reanalysis from the European Center for Medium-Range Weather Forecasts (ERA5; Hersbach *et al* 2020). The data we examined have a horizontal resolution of $1.5^\circ \times 1.5^\circ$ and cover the period of 1950–2021. We focus on the boreal winter from December to February. After detrending, the anomalies are obtained by removing the seasonal cycle, which is defined as the time mean and first two harmonics of the full-year climatology.

We also examine climate models from the Coupled Model Intercomparison Project Phase 6 (CMIP6). We select 16 models that are shown to realistically simulate the QBO (Richter *et al* 2020, Zuo *et al* 2022, Rao *et al* 2023). The historical simulations we examined cover the period of 1950–2014. All model data are bilinearly interpolated to a $1.5^\circ \times 1.5^\circ$ common grid. Only one member from each model is used. The list of CMIP6 models and the ensemble members used are shown in table S1.

Since the QBO in climate models has a weak amplitude at 50 hPa compared to reanalysis, here the QBO is indexed using the standardized seasonal 10 hPa zonal wind that is averaged between 5° S and 5° N (Elsbury *et al* 2021a). This works because of the anticorrelation between 10 hPa and 50 hPa QBO winds (Richter *et al* 2020, Anstey *et al* 2022b). We define a wQBO year when the QBO index is smaller than -0.5 and an eQBO year when the index is larger than 0.5. According to this definition, there are 28 eQBO and 31 wQBO years in ERA5. The numbers of QBO years in each model are listed in table S1. The main conclusions are not sensitive to the chosen QBO indexing scheme.

2.2. Definition of strong stratospheric wave events

We identify strong stratospheric wave events based on the empirical orthogonal function (EOF) analysis of the 10 hPa geopotential height, for ERA5 and each model individually (Ding *et al* 2023a, 2023b). While the lower stratosphere is more strongly related to tropospheric variability, using the 10 hPa field makes it more straightforward to identify the contribution of stratospheric variability to tropospheric weather. EOF analysis is applied to the zonally asymmetric geopotential height (removing the zonal mean) north of 20° N, weighted by the square root of the cosine of latitude. We note that the leading EOF pattern encompasses the variability from all zonal wave numbers. The standardized principal component of the leading EOF mode is taken as the stratospheric planetary wave index, largely describing the strength of the planetary wave-1 in the stratosphere. While wave-2 patterns from other EOFs may also have important implications (e.g. Charlton and Polvani 2007), we focus on the wave-1 pattern from the leading EOF due to its predominant explained variance (Ding *et al* 2023a). A strong stratospheric wave event is identified as the consecutive days when the planetary wave index is above its 95th percentile. No minimum duration is required. Day 0 refers to the first day meeting the threshold.

The strong stratospheric wave events are subsampled based on the QBO phase of the winter in which the event occurs. In ERA5, this results in a frequency of 1.23 strong wave events per year during wQBO years (38 events in total) and 0.75 events per year during eQBO years (21 events in total). The CMIP6 ensemble produces, on average, 1.07 strong wave events per wQBO year (451 events in total) and 0.98 events per eQBO year (414 events in total). The numbers of strong wave events in each model are listed in table S1.

2.3. Plumb wave activity flux

We calculate the Plumb wave activity flux to describe the 3D propagation of planetary waves (Plumb 1985)

$$\{F^{\lambda}, F^{\phi}, F^{z}\} = p\cos(\phi)\left\{v'^2 - \frac{1}{fa\cos(\phi)}\frac{\partial(v'\Phi')}{\partial\lambda}, -u'v' + \frac{1}{fa\cos(\phi)}\frac{\partial(u'\Phi')}{\partial\lambda}, \right.$$
$$\left. \frac{f}{\partial\tilde{T}/\partial z + \kappa\tilde{T}/H}\left[v'T' - \frac{1}{fa\cos(\phi)}\frac{\partial(T'\Phi')}{\partial\lambda}\right]\right\}$$

where λ is longitude, ϕ is latitude, z is height, and p is pressure. T is temperature, Φ is geopotential height, u is the zonal wind, and v is the meridional wind. f is the Coriolis parameter and a is Earth's radius. κ is the specific gas constant of dry air divided by the specific heat of dry air. $\tilde{T}$ is the domain-averaged temperature. H is the log-pressure scale height. Primes denote the deviations from zonal means.

It is noteworthy that the upward propagation of planetary waves can also be inferred from the westward tilt of geopotential height anomalies with increasing altitude. While the direction of the wave tilt for the composite of height anomalies implies the sign of transient eddy fluxes, Plumb fluxes include both transient eddy fluxes and the interference between transient and climatological planetary waves.

3. Results

3.1. QBO modulates the surface signal of strong stratospheric wave events in reanalysis

We first compare the evolution of circulation patterns during strong stratospheric wave events for the two QBO phases in ERA5 (figure 1). The 10 hPa geopotential height anomalies linked to strong stratospheric wave events during wQBO and eQBO years share similar patterns, featuring an NA ridge and a Eurasian trough (figures 1(a) and (b)). This wave-1 pattern is largely in phase with the wave-1 climatology and reinforces the climatological wave-1 via constructive wave interference (Smith and Kushner 2012, Ding *et al* 2022). We note that on day 10, the ridge anomaly under eQBO is slightly stronger compared to that under wQBO, implying a more persistent NA ridge associated with eQBO strong wave events. The zonal mean component of their differences corresponds to a positive NAM (figure 1(c)), which is attributable to the QBO effect on the seasonal mean polar vortex and diminishes after removing winter means (figure S1). However, removing this QBO modulation on winter means does not affect the tropospheric signals to be described below (figures S1 and S2), suggesting that the impact of QBO on strong wave events acts on a shorter timescale than its influence on the polar vortex. For 500 hPa composites, strong stratospheric wave events under different QBO phases are similar before and around the event onset (days −5–0), showing a strong Alaskan trough and two ridges over eastern North America and Europe (figures 1(a) and (b)). These observed precursor patterns match the ones associated with strong wave events during all the winters regardless of QBO phases and also resemble the pattern during negative eddy heat flux events (Shaw and Perlwitz 2013, Ding *et al* 2023a). However, on day 10, wQBO strong wave events show a northern North Pacific ridge and an NA trough while eQBO events display a northern North Pacific trough. This is more clearly shown in the differences between wQBO and eQBO (figure 1(c)). The opposite signs of the northern North Pacific anomalies may explain the negligible tropospheric signal over the North Pacific when considering all the winters (see figure 2 in Ding *et al* 2023a). In other words, the tropospheric precursor transitions into an opposite pattern during wQBO strong wave events while the precursor is maintained through the lifecycle of eQBO events.

The related surface signals during wQBO and eQBO are consistent with the mid-tropospheric circulation anomalies. The composite of wQBO strong wave events features a transition from warm anomalies over North America before the event onset to cold anomalies on day 10 (figure 2(a)). This temperature swing coincides with a shift from a cyclonic anomaly in sea level pressure (SLP) over Alaska to an anticyclonic anomaly 5–10 d later. These surface signatures during wQBO are largely in line with those during all the winters, except for the Alaskan anticyclonic anomaly (Ding *et al* 2023b). On the other hand, the surface composite of eQBO strong wave events is characterized by a persistent cyclonic anomaly over Alaska (figure 2(b)). This induces warm anomalies over North America and mitigates the temperature drop. We note that the warm signal on day 10 is insignificant, accompanied by some cooling around Davis Strait and the west coast of the United States. Interestingly, the SLP anomalies over the Atlantic project onto the positive North Atlantic Oscillation (NAO) regardless of the QBO phase, consistent with the results during all the winters. It is worth noting that these surface signals following strong wave events are distinct from those related to anomalous polar vortex events (Ding *et al* 2022, 2023a, Messori *et al* 2022). This result also aligns with the finding that the weather regime most sensitive to the polar vortex strength is not the most important for NA cold extremes (Lee *et al* 2019). While the temperature drop over North America has been connected

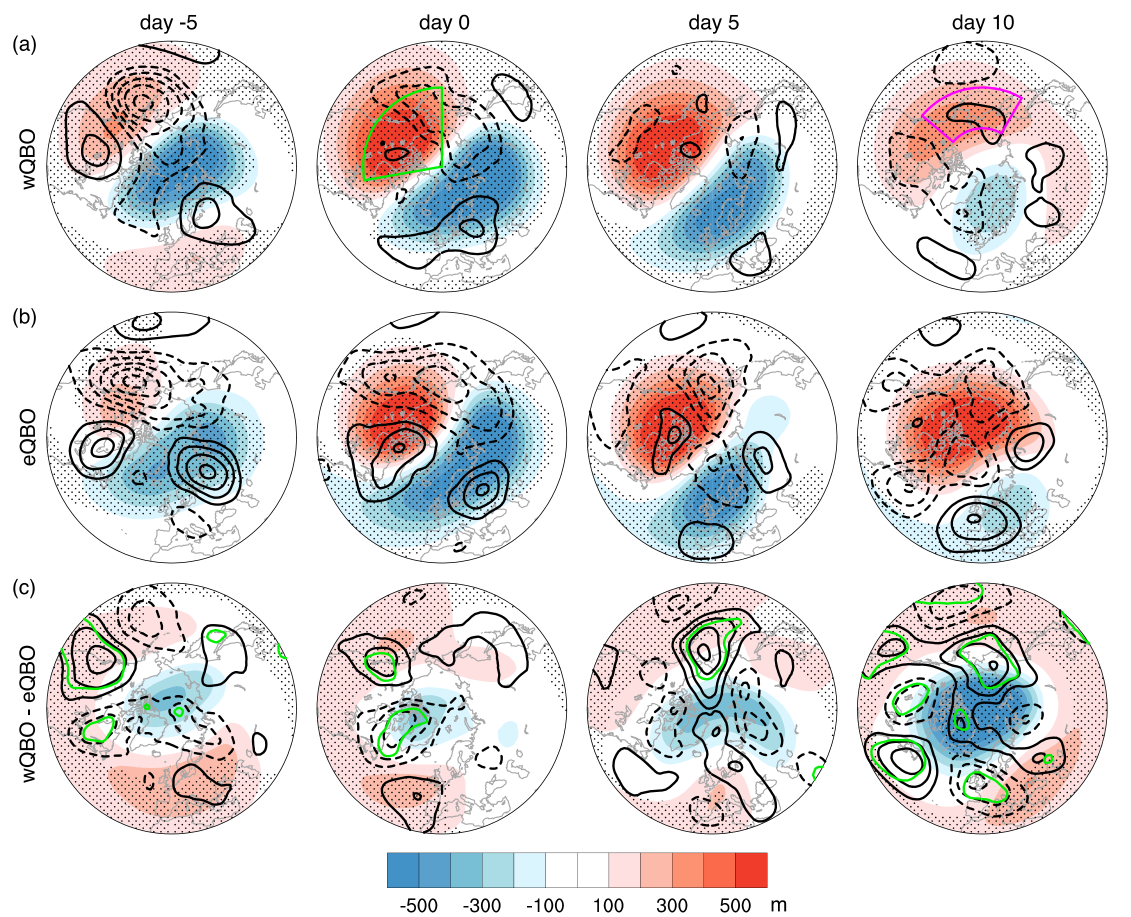

Figure 1. Composites of geopotential height anomalies at 10 hPa (Z10, shading) and 500 hPa (Z500, contours, 25 m interval) on day −5, 0, 5, and 10 for strong stratospheric wave events in ERA5 under wQBO (a) and eQBO (b). (c) Differences between (a) and (b). Stippling in (a), (b) denotes the regions where the shaded anomalies are significant at the 95% confidence level based on the two-sided Student's *t*-test. Stippling and green contours in (c) denote 95% significant Z10 and Z500 differences based on the two-sided Welch's unequal variances *t*-test. The time evolution is smoothed by a 5-day running average. Day −5 represents the average between day −7 and day −3. The green box in (a) (50°–90° N, 80° W–180°) indicates the region where stratospheric ridge anomalies are calculated, and the magenta box (50°–70° N, 150° E–130° W) indicates the region of tropospheric northern North Pacific anomalies. See figure S1 for the results after removing seasonal means.

to the stratosphere through wave coupling (Guan *et al* 2020, Messori *et al* 2022, Shen *et al* 2022, Ding *et al* 2023b), figure 2 suggests a more nuanced picture of this connection that depends on the QBO phase.

Vertical wave structures associated with strong stratospheric wave events under different QBO phases are compared by using zonally asymmetric geopotential height anomalies and Plumb flux anomalies averaged over 50°–70° N (figure 3). Before and around the onset, strong wave events under wQBO and eQBO both show upward and eastward Plumb flux anomalies over Siberia, reinforcing the stratospheric ridge over North America (figures 3(a) and (b)). Accordingly, the geopotential height anomalies and their wave-1 components (black lines in figure 3) are characterized by a westward phase tilt with altitude. Around day 5 to day 10, wQBO strong wave events feature a shift to an eastward tilt, coinciding with the downward Plumb flux anomalies over North America (figure 3(a)). This wave phase alteration is consistent with the results using all the winters, which may be thought of as an indication of local wave reflection (Holton and Mass 1976, Perlwitz and Harnik 2003, Ding *et al* 2023a). However, a westward tilt of geopotential height anomalies persists throughout strong wave events during eQBO (figure 3(b)). In addition, we confirm that the wave structures remain consistent after removing seasonal means, regardless of whether the winter mean effect of the QBO is included (cf figure 3 vs. figure S3).

From a perspective of weather systems, wQBO strong wave events are followed by a weakening of the stratospheric NA ridge, which descends and forms an anomalous ridge over the northern North Pacific in the troposphere (figure 3(a)), reminiscent of the evolution during planetary wave reflection (Kodera *et al* 2013). This also leads to the development of an NA trough downstream that favors cold air advection (figure 1). In contrast, the NA ridge is largely confined in the stratosphere following eQBO strong wave events while the northern North Pacific is occupied by a tropospheric trough (figure 3(b)).

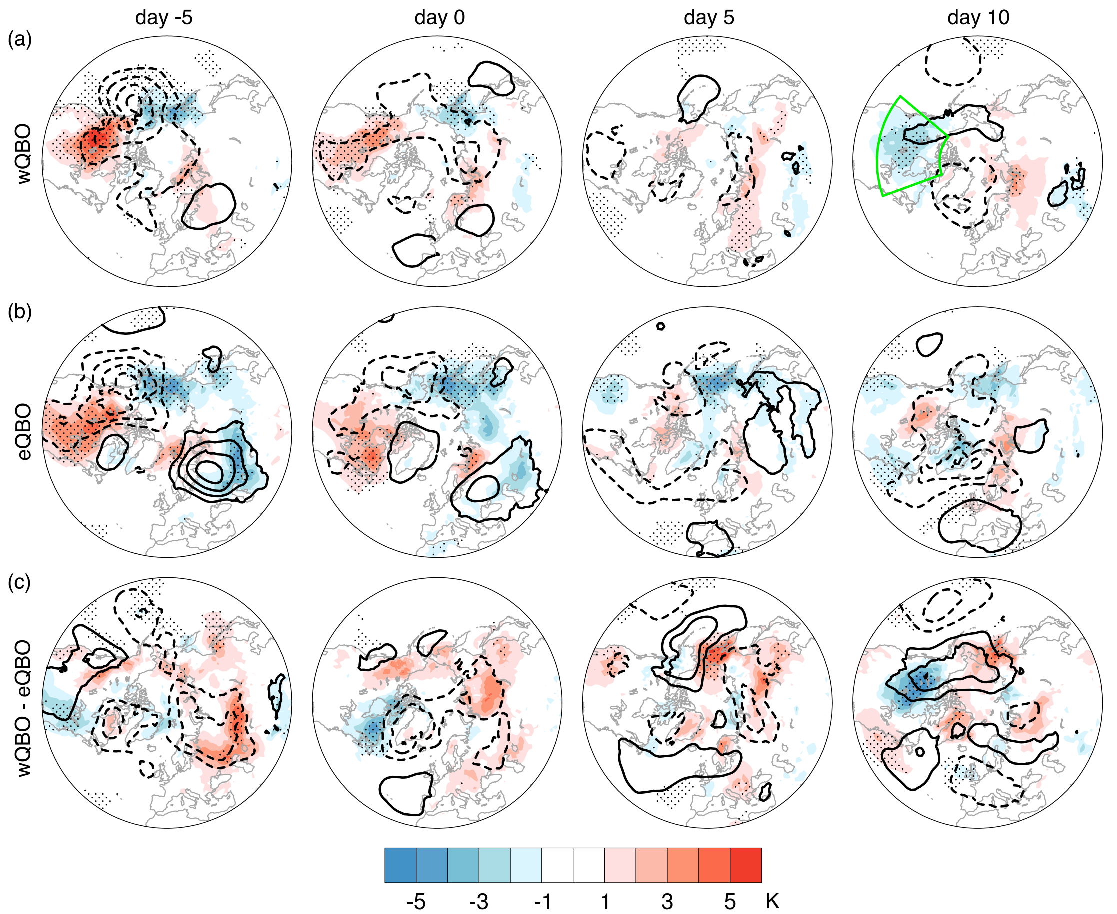

Figure 2. Composites of surface air temperature (SAT, shading) and SLP (contours, 2.5 hPa interval) on day −5, 0, 5, and 10 for strong stratospheric wave events in ERA5 under wQBO (a) and eQBO (b). (c) Differences between (a) and (b). Stippling in (a), (b) denotes the regions where the shaded anomalies are significant at the 95% confidence level based on the two-sided Student's *t*-test. Stippling in (c) denotes 95% significant differences based on the two-sided Welch's unequal variances *t*-test. The time evolution is smoothed by a 5-day running average. Day −5 represents the average between day −7 and day −3. The green box in (a) (40°–70° N, 70° W–130° W) indicates the region of NA SAT anomalies. See figure S2 for the results after removing seasonal means.

We also examine zonally averaged zonal winds during strong wave events under wQBO and eQBO (figure S4). While they both show zonal wind deceleration in the extratropical region, only strong wave events under wQBO are associated with a vertical dipole structure around day 0, marked by significant negative anomalies in the upper stratosphere and positive anomalies below (figure S4(a)). This dipole pattern implies a potential reflective surface of planetary waves (Perlwitz and Harnik 2003). Besides, despite the increased upward wave propagation, wQBO strong wave events do not show negative zonal wind anomalies in high latitudes like eQBO strong wave events (figure S4), suggesting that the waves are not absorbed in the stratosphere. Figure S5 shows that the stratospheric zonal wind speed decreases with altitude around the onset of strong wave events during wQBO (blue line), further indicating the formation of a vertical reflective surface (Perlwitz and Harnik 2003). These results imply that wQBO induces a favorable condition for vertical wave reflection, leading to the vertical structure shift and subsequent cold advection over North America following strong wave events (figures 2 and 3).

In summary, reanalysis indicates that the QBO phase modulates the surface signal of strong stratospheric wave events, with an increased risk of cold extremes over North America during wQBO but a muted risk during eQBO.

3.2. CMIP6 models lack the sensitivity of strong stratospheric wave events to the QBO

It is then interesting to ask whether climate models can capture the dependence of the vertical wave coupling on the QBO phase. To this end, we compare the time series of stratospheric and tropospheric indices under different QBO phases in ERA5 and CMIP6 (figure 4). The regionally averaged 10 hPa geopotential height anomalies over northern North America (50°–90° N, 80° W–180°) are compared with 500 hPa anomalies over the northern North Pacific (50°–70° N, 150° E–130° W). We select these regions due to the contrast between wQBO and eQBO events and linkages to NA cold anomalies (figures 1 and 2). Following strong

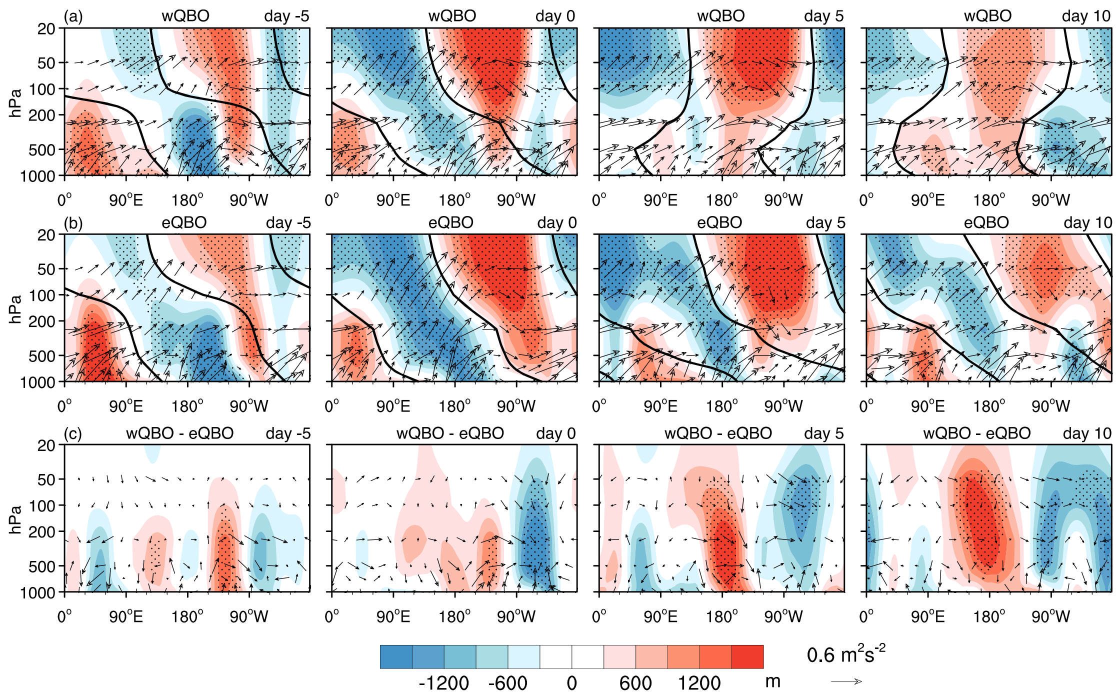

Figure 3. Vertical wave coupling associated with strong stratospheric wave events during wQBO and eQBO in ERA5. (a) Composites of the zonally asymmetric component of anomalous geopotential height (shading) and vertical and zonal components of anomalous Plumb wave activity flux (vector) averaged over 50°–70° N on day −5, 0, 5, and 10 for strong wave events under wQBO. (b) As in (a), but for strong wave events under eQBO. (c) Differences between (a) and (b). Black lines are zero contours of the wave-1 component of anomalous geopotential height, indicating the vertical phase tilt of wave-1. Stippling in (a), (b) denotes the regions where the shaded anomalies are significant at the 95% confidence level based on the two-sided Student's t-test. Stippling in (c) denotes 95% significant differences based on the two-sided Welch's unequal variances t-test. The time evolution is smoothed by a 5-day running average. Day −5 represents the average between day −7 and day −3. To account for the smaller air density with decreasing pressure, the magnitude of the Plumb flux is scaled by $(1000/p)^{1/2}$, and geopotential height is scaled by $(p/1000)^{1/2}$, where p is pressure. The vertical component of the Plumb flux is also scaled by a factor of 200. See figure S3 for the results after removing seasonal means. See figure S6 for the total (zonally asymmetric + zonal mean) field of anomalous geopotential height and absolute (anomalous + climatological) Plumb flux.

wave events under wQBO, the CMIP6 multi-model ensemble (MME) mean (red lines in figure 4) shows a slightly more persistent stratospheric NA ridge compared to ERA5 (figure 4(a)). As for the troposphere, the CMIP6 MME presents virtually no anomalies over the northern North Pacific in contrast to an attenuated Aleutian Low in ERA5 during days 5–20 noted by the weakly positive anomalies (figure 4(c)). The difference between CMIP6 and ERA5 under eQBO is generally the opposite but with larger amplitudes: the stratospheric NA ridge weakens during days 5–20 in CMIP6 while it sustains in ERA5 (figure 4(b)). This is in line with the results that remove the seasonal mean effect of the QBO (figure S8). In the troposphere, CMIP6 shows negligible anomalies though ERA5 exhibits a significantly strengthened Aleutian Low (figure 4(d)). A similar comparison between CMIP6 and ERA5 can be drawn from circulation patterns (cf figure 1 vs. figure S7). These results suggest that the evolution of the stratospheric northern NA ridge after the onset is connected to strong wave events' tropospheric signals over the northern North Pacific. Moreover, CMIP6 models seem to lack the sensitivity of this connection to QBO phases which is observed in ERA5.

Of particular interest is the linkage between strong stratospheric wave events and cold extremes over North America. Figures 4(e) and (f) present the Probability Density Function (PDF) of NA surface air temperature (SAT) (40°–70° N, 70° W–130° W) anomalies during days 5–20 after strong wave events under wQBO and eQBO. In ERA5, wQBO strong wave events feature a general shift towards colder temperatures that is 95% significant based on the two-tailed two-sample Kolmogorov–Smirnov (KS) test, whereas eQBO events show little change (figure 4(e)). The extreme cold risk is further quantified by the risk ratio for the exceedance frequency below a certain standard deviation (SD) of the PDF. Compared to all the winter days, wQBO strong wave events increase the risk of exceeding −1, −1.5, and −2 SD below climatology by 50%, 80%, and 110%, which is higher than those of strong wave events during all the winters (Ding *et al* 2023b). Strong wave events during eQBO, on the contrary, decrease the cold extreme risk of exceeding −1.5 and −2 SD by 10% and 60%. These divergent cold risks under wQBO and eQBO match the observed patterns (figure 2). However, the CMIP6 PDFs during wQBO and eQBO both indicate a statistically significant shift toward colder anomalies based on the KS test (figure 4(f)). Consistent results are found in the risk ratios for

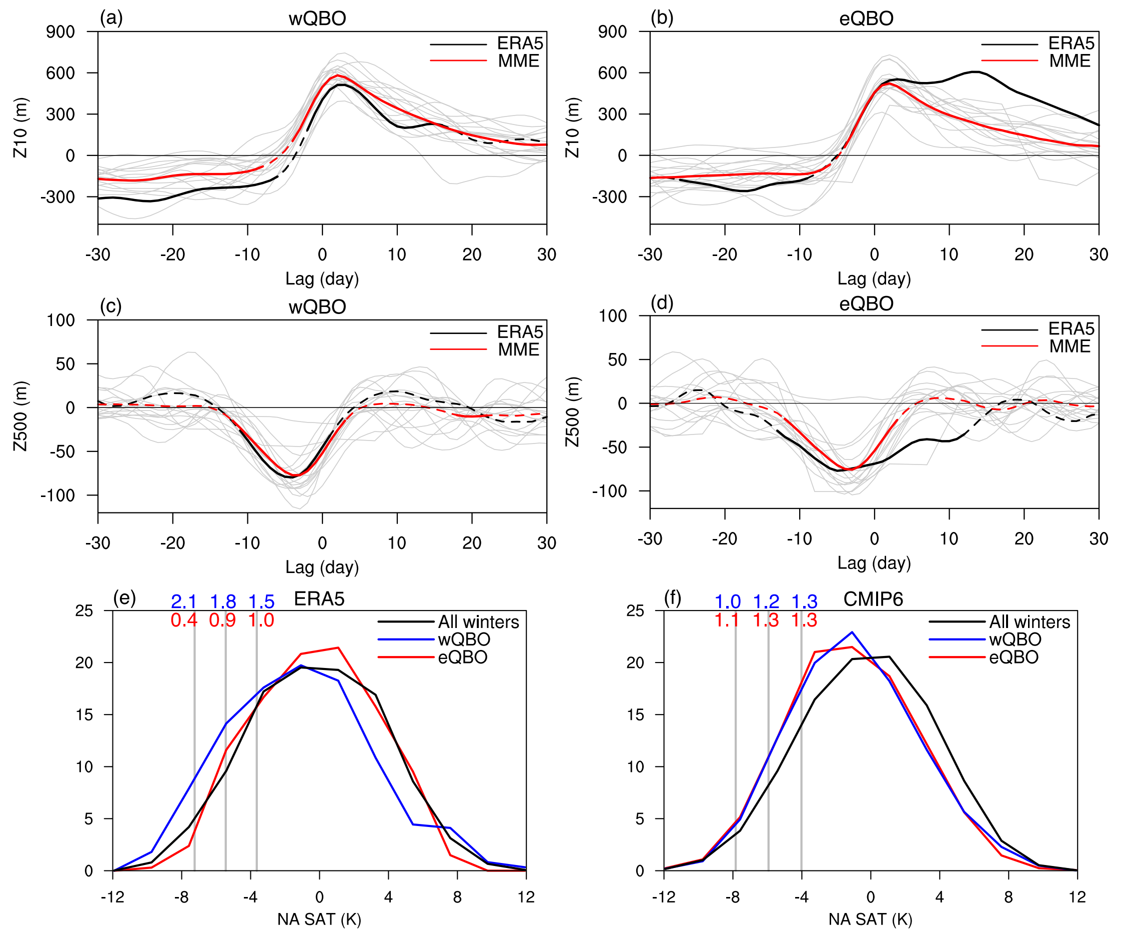

Figure 4. Evolution of circulation anomalies and risks of NA cold extremes linked to strong stratospheric wave events. (a)–(b) Composites of 10 hPa geopotential height anomalies averaged over northern North America (50°–90° N, 80° W–180°) for strong wave events under wQBO (a) and eQBO (b). See figure S8 for the results after removing seasonal means. (c)–(d) As in (a)–(b), but for 500 hPa geopotential height anomalies averaged over the northern North Pacific (50°–70° N, 150° E–130° W). ERA5 is denoted by black lines, the CMIP6 multi-model ensemble (MME) is in red, and individual models are in gray. Solid parts of the lines for ERA5 and CMIP6 MME indicate the anomalies significant at the 95% confidence level based on the two-sided Student's t-test. (e)–(f) Probability density function (PDF) of NA SAT (40°–70° N, 70° W–130° W) anomalies during days 5–20 following strong wave events under wQBO (blue lines) and eQBO (red lines) in ERA5 (e) and CMIP6 (f). The vertical gray lines denote −1, −1.5, and −2 SD of NA SAT anomalies in all the winter days, and the values in blue (red) depict the risk ratios of the exceedance frequency following strong wave events under wQBO (eQBO).

exceedance frequency, showing virtually no differences between wQBO and eQBO (1.3, 1.3, 1.1 vs. 1.3, 1.2, 1.0). These results suggest that CMIP6 models simulate a biased surface signature following strong stratospheric wave events under eQBO, with the NA cold signals being too strong compared to ERA5. These findings are also confirmed by the temporal evolution of NA SAT (figure S9). In figure S9, we also note that strong wave events under eQBO are followed by significant NA cold anomalies with a 20 day lag. However, the associated SLP pattern is different from that on day 10 after wQBO strong wave events, which features positive NAO over the Atlantic (figure S10). In addition, the anomalies on day 20 are isolated and confined to the troposphere (figure S11(b)). These results suggest that the NA cold anomalies following eQBO strong wave events with a 20 day lag are not directly related to the surface response to strong wave events analyzed in this study.

An outstanding question is whether the biased cooling signature of strong stratospheric wave events can be linked to the stratospheric representation. Ding *et al* (2023a) demonstrated that models with a degraded representation of stratospheric wave structure tend to exhibit biases in the surface signals of strong wave events. Our analysis reveals that, following the onset of eQBO strong wave events, the CMIP6 MME simulates a stratospheric wave pattern that diverges from the ERA5 results (figure 4(b)). This discrepancy prompts us to consider if differences in the stratospheric ridge evolution are linked to the varied tropospheric signals across models. To investigate this potential connection, figure 5 presents a scatterplot for the changes in the stratospheric northern NA ridge (between days 5–20 and days −5–5) versus tropospheric anomalies over the northern North Pacific during days 5–20 across CMIP6 models. There is a statistically significant linear correlation for both strong wave events during wQBO ($r = -0.51$) and events during eQBO

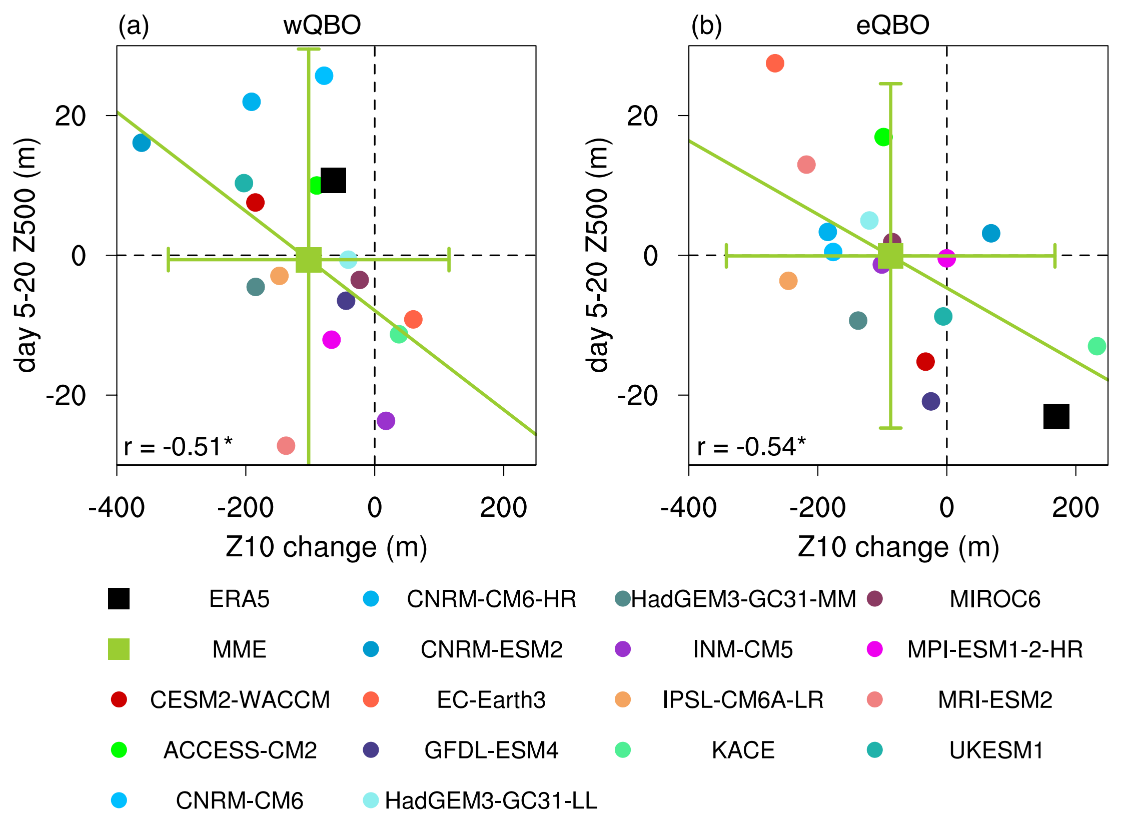

Figure 5. Intermodel scattering between stratospheric and tropospheric indices associated with strong stratospheric wave events. (a) 500 hPa northern North Pacific anomalies during days 5–20 versus the change of 10 hPa northern NA geopotential height anomalies between days 5–20 and days −5–5 under wQBO. (b) As in (a), but for eQBO. ERA5 is denoted as black squares, the CMIP6 MME means in green, and individual models are noted in the legend. The colored lines show linear regressions for CMIP6, with correlation coefficients (r) given in the legend. The error bars show the ±2 SD of CMIP6. Asterisks denote coefficients significant at the 95% confidence level based on the two-sided Student's t-test.

($r = -0.54$), consistent with the finding that a cyclonic anomaly over the northern North Pacific tends to enhance upward wave propagation (e.g. Garfinkel *et al* 2010, Woollings *et al* 2010). We caution that the correlations for the vertical wave coupling may involve interactions with changes in the stratospheric polar vortex (Kolstad *et al* 2010, Domeisen *et al* 2020, Lawrence *et al* 2020, Huang *et al* 2021) or the Madden–Julian oscillation (MJO; Johnson *et al* 2014) during different QBO phases, but isolating all the factors of climate variability is beyond the scope of the present study.

This intermodel relation supports that a more pronounced weakening of the stratospheric ridge after strong wave events correlates with tropospheric anticyclonic anomalies over the North Pacific, inducing NA cold anomalies (figure 4). The CMIP6 MME (green squares in figure 5) shows negligible differences between wQBO and eQBO. Interestingly, ERA5 strong wave events during eQBO approach the uncertainty limit (2 SD) of CMIP6, whereas ERA5 events during wQBO align closely with the CMIP6 MME. This suggests that the discrepancy between CMIP6 and ERA5 cannot be fully explained by internal variability which is part of model uncertainties. The stratospheric and tropospheric signals following strong wave events in climate models are systematically biased for eQBO, leading to models' insensitivity to QBO phases after strong stratospheric wave events. We also note that the stratospheric zonal wind in ERA5 strongly decelerates after eQBO strong wave events, while it remains relatively unchanged in the CMIP6 MME (figure S12). This is consistent with models' known tendency to underpredict the weakening of the polar vortex associated with eQBO (e.g. Elsbury *et al* 2021a).

4. Conclusions

In this paper, we have investigated how the surface conditions following extreme stratospheric events may depend on the QBO phase, by comparing strong stratospheric wave events during wQBO and eQBO years. In contrast to most previous studies on the QBO that were focused on the role of SSWs in modulating the risk of cold extremes at the surface (e.g. Rao *et al* 2020), this study sheds light on an alternative stratospheric pathway through vertical wave coupling. During wQBO, strong wave events are followed by a northern North Pacific ridge in the troposphere, increasing cold risks over North America. Conversely, strong wave events under eQBO show a persistent tropospheric trough throughout the lifecycle, resulting in muted NA cold risks. Accordingly, the vertical structure shifts from a westward phase tilt to an eastward tilt during wQBO events while remaining at a westward tilt during eQBO events. This dynamic insight may prove beneficial for subseasonal predictions of cold extremes when integrated with other factors such as the El Nino–Southern Oscillation (ENSO; Kenyon and Hegerl 2008, Xiang *et al* 2019, Albers *et al* 2022), the stratospheric polar vortex (Kolstad *et al* 2010, Domeisen *et al* 2020, Lawrence *et al* 2020, Huang *et al* 2021, Scaife *et al* 2022), and the MJO (Johnson *et al* 2014). We also note that this pathway differs from the established connection between the QBO and the NA coldness through SSWs, as strong stratospheric wave events are distinct from SSWs in terms of surface impacts and mechanisms (Ding *et al* 2022, 2023a, Messori *et al* 2022). Therefore, a comprehensive comparison of different pathways of QBO's influences on surface weather warrants future research.

Although eQBO tends to induce a weak polar vortex, there are more strong stratospheric wave events during wQBO (38 events) than during eQBO (21 events). This discrepancy may be reconciled by different timescales of these events. The stratosphere-troposphere coupling of strong wave events acts on a shorter timescale compared with an anomalous polar vortex (Ding *et al* 2022). In addition, strong wave events are preceded by a stronger-than-normal polar vortex, which may be related to the stratospheric preconditioning for upward wave activity (McIntyre 1982, Ding *et al* 2022). Thus, the seasonally stronger polar vortex during wQBO may provide a favorable condition for strong wave events and vertical wave reflection. This wave reflection involves both the seasonal mean effect of the QBO (a strong polar vortex) and subseasonal variabilities (strong stratospheric wave activity). We have also examined the sea surface temperature (SST) anomalies associated with strong wave events (figure S13), consistent with the SST patterns linked to the QBO (Randall *et al* 2023). The implications of these SST anomalies on planetary waves require further investigation.

The QBO impact on strong stratospheric wave events is further examined in QBO-resolving CMIP6 models. We found that models do not replicate the distinct surface signatures under different QBO phases observed in reanalysis, suggesting a lack of sensitivity to QBO phases in climate models. Instead, the models consistently show an increased risk in NA cold following strong wave events during both wQBO and eQBO years. The lack of QBO dependence is linked to the absence of tropospheric anomalies over the northern North Pacific. This may be attributed to biases in the evolution of the stratospheric ridge following eQBO strong wave events. Similarly, the persistence of stratospheric anomalies following SSWs has been suggested to strongly influence their tropospheric impact (Maycock and Hitchcock 2015). In addition, many models exhibit an unrealistic reduction in upward wave fluxes in the lower stratosphere (Wu and Reichler 2020). Our results imply that models have biases of excessive downward coupling under eQBO, which may contribute to this issue. The root cause behind the model's insensitivity of strong wave events to the QBO phase warrants future investigation, potentially including considerations of the QBO structure (Kim *et al* 2020), model climatology (Karpechko *et al* 2021), and lid height and vertical resolution (Shaw *et al* 2014, Wu and Reichler 2020).

Our results add to the growing body of research on the QBO's global impacts. Previous literature has documented that the stratosphere's downward influence is sensitive to various factors modulating planetary waves, such as ENSO (Butler and Polvani 2011, Domeisen *et al* 2019), topography (Gerber and Polvani 2009, Garfinkel *et al* 2020, Wang *et al* 2023), and sea ice (Kim *et al* 2014, Sun *et al* 2015). Our analysis has demonstrated that the surface signature of strong stratospheric wave events and the associated cold extreme risk over North America depends on the phase of the QBO. In this regard, while a few studies have shown that downward wave reflection is susceptible to SST, solar activity, and sea ice (Lubis *et al* 2016, Lu *et al* 2017, Zou and Zhang 2024), much work is needed to understand the sensitivity of extreme stratospheric wave activity to various factors of climate variability. Findings from our paper could potentially enhance forecasting of severe winter cold in the U.S. and Canada, benefiting transportation, energy management, and public health by enabling better preparedness and resource allocation (Vajda *et al* 2014, Charlton-Perez *et al* 2019, Perera *et al* 2020).

Data availability statement

The ERA5 reanalysis is available at https://cds.climate.copernicus.eu/cdsapp#!/dataset/reanalysis-era5-pressure-levels?tab=form. The CMIP6 outputs used in this study can be obtained from the CMIP archive at https://esgf-node.llnl.gov/projects/esgf-llnl. A list of CMIP6 models used can be found in table S1.

Acknowledgments

We acknowledge the WCRP Working Group on Coupled Modeling which is responsible for the CMIP. We also acknowledge high-performance computing support from Cheyenne (https://doi.org/10.5065/D6RX99HX) provided by NCAR's Computational and Information Systems Laboratory, sponsored by the National Science Foundation. G C is supported by the U.S. NSF Grant AGS-2232581 and NASA Grant 80NSSC21K1522. The authors declare that they have no competing interests.

ORCID iDs

Xiuyuan Ding https://orcid.org/0000-0001-6743-6480
Gang Chen https://orcid.org/0000-0003-4934-1909
Gudrun Magnusdottir https://orcid.org/0000-0001-6079-5886

References

Albers J R, Newman M, Hoell A, Breeden M L, Wang Y and Lou J 2022 The February 2021 cold air outbreak in the united states: a subseasonal forecast of opportunity *Bull. Am. Meteorol. Soc.* **103** E2887–904
Andrews M B, Knight J R, Scaife A A, Lu Y, Wu T, Gray L J and Schenzinger V 2019 Observed and simulated teleconnections between the stratospheric quasi-biennial oscillation and northern hemisphere winter atmospheric circulation *J. Geophys. Res. Atmos.* **124** 1219–32
Anstey J A *et al* 2022b Teleconnections of the Quasi-Biennial oscillation in a multi-model ensemble of QBO-resolving models *Q. J. R. Meteorol. Soc.* **148** 1568–92
Anstey J A, Osprey S M, Alexander J, Baldwin M P, Butchart N, Gray L, Kawatani Y, Newman P A and Richter J H 2022a Impacts, processes and projections of the quasi-biennial oscillation *Nat. Rev. Earth Environ.* **3** 588–603
Baldwin M P *et al* 2001 The quasi-biennial oscillation *Rev. Geophys.* **39** 179–229
Baldwin M P *et al* 2021 Sudden stratospheric warmings *Rev. Geophys.* **59** e2020RG000708
Baldwin M P and Dunkerton T J 2001 Stratospheric harbingers of anomalous weather regimes *Science* **294** 581–4
Blackport R, Screen J A, van der Wiel K and Bintanja R 2019 Minimal influence of reduced Arctic sea ice on coincident cold winters in mid-latitudes *Nat. Clim. Change* **9** 697–704
Butler A H and Polvani L M 2011 El Niño, La Niña, and stratospheric sudden warmings: a reevaluation in light of the observational record *Geophys. Res. Lett.* **38** L13807
Charlton A J and Polvani L M 2007 A new look at stratospheric sudden warmings. Part I: climatology and modeling benchmarks *J. Clim.* **20** 449–69
Charlton-Perez A J, Aldridge R W, Grams C M and Lee R 2019 Winter pressures on the UK health system dominated by the greenland blocking weather regime *Weather Clim. Extremes* **25** 100218
Cohen J, Agel L, Barlow M and Entekhabi D 2023 No detectable trend in mid-latitude cold extremes during the recent period of Arctic amplification *Commun. Earth Environ.* **4** 1–9
Cohen J, Agel L, Barlow M, Garfinkel C I and White I 2021 Linking Arctic variability and change with extreme winter weather in the United States *Science* **373** 1116–21
Davis N A, Richter J H, Glanville A A, Edwards J and LaJoie E 2022 Limited surface impacts of the January 2021 sudden stratospheric warming *Nat. Commun.* **13** 1136
Ding X, Chen G and Ma W 2023a Stratosphere-troposphere coupling of extreme stratospheric wave activity in CMIP6 models *J. Geophys. Res. Atmos.* **128** e2023JD038811
Ding X, Chen G, Sun L and Zhang P 2022 Distinct North American cooling signatures following the zonally symmetric and asymmetric modes of winter stratospheric variability *Geophys. Res. Lett.* **49** e2021GL096076
Ding X, Chen G, Zhang P, Domeisen D I V and Orbe C 2023b Extreme stratospheric wave activity as harbingers of cold events over North America *Commun. Earth Environ.* **4** 187
Domeisen D I V *et al* 2020 The role of the stratosphere in subseasonal to seasonal prediction: 2. predictability arising from stratosphere-troposphere coupling *J. Geophys. Res. Atmos.* **125** e2019JD030923
Domeisen D I V, Garfinkel C I and Butler A H 2019 The teleconnection of El Niño Southern oscillation to the stratosphere *Rev. Geophys.* **57** 5–47
Elsbury D, Peings Y and Magnusdottir G 2021a CMIP6 models underestimate the Holton-Tan effect *Geophys. Res. Lett.* **48** e2021GL094083
Elsbury D, Peings Y and Magnusdottir G 2021b Variation in the Holton–Tan effect by longitude *Q. J. R. Meteorol. Soc.* **147** 1767–87
Garfinkel C I, Hartmann D L and Sassi F 2010 Tropospheric precursors of anomalous Northern Hemisphere stratospheric polar vortices *J. Clim.* **23** 3282–99
Garfinkel C I, White I, Gerber E P, Jucker M and Erez M 2020 The building blocks of Northern Hemisphere wintertime stationary waves *J. Clim.* **33** 5611–33
Gerber E P and Polvani L M 2009 Stratosphere–troposphere coupling in a relatively simple AGCM: the importance of stratospheric variability *J. Clim.* **22** 1920–33
Guan W, Jiang X, Ren X, Chen G, Lin P and Lin H 2020 The leading intraseasonal variability mode of wintertime surface air temperature over the North American sector *J. Clim.* **33** 9287–306
Harnik N, Messori G, Caballero R and Feldstein S B 2016 The circumglobal North American wave pattern and its relation to cold events in eastern North America *Geophys. Res. Lett.* **43** 11015–23
Hartmann D L 2015 Pacific sea surface temperature and the winter of 2014 *Geophys. Res. Lett.* **42** 1894–902
Hersbach H *et al* 2020 The ERA5 global reanalysis *Q. J. R. Meteorol. Soc.* **146** 1999–2049

Holton J R and Mass C 1976 Stratospheric vacillation cycles *J. Atmos. Sci.* **33** 2218–25

Holton J R and Tan H-C 1980 The influence of the equatorial Quasi-Biennial oscillation on the global circulation at 50 mb *J. Atmos. Sci.* **37** 2200–8

Huang J, Hitchcock P, Maycock A C, McKenna C M and Tian W 2021 Northern hemisphere cold air outbreaks are more likely to be severe during weak polar vortex conditions *Commun. Earth Environ.* **2** 147

Johnson N C, Collins D C, Feldstein S B, L'Heureux M L and Riddle E E 2014 Skillful wintertime North American temperature forecasts out to 4 weeks based on the state of ENSO and the MJO *Weather Forecast.* **29** 23–38

Johnson N C, Xie S-P, Kosaka Y and Li X 2018 Increasing occurrence of cold and warm extremes during the recent global warming slowdown *Nat. Commun.* **9** 1724

Karpechko A Y, Tyrrell N L and Rast S 2021 Sensitivity of QBO teleconnection to model circulation biases *Q. J. R. Meteorol. Soc.* **147** 2147–59

Kenyon J and Hegerl G C 2008 Influence of modes of climate variability on global temperature extremes *J. Clim.* **21** 3872–89

Kim B-M, Son S-W, Min S-K, Jeong J-H, Kim S-J, Zhang X, Shim T and Yoon J-H 2014 Weakening of the stratospheric polar vortex by Arctic sea-ice loss *Nat. Commun.* **5** 4646

Kim H, Caron J M, Richter J H and Simpson I R 2020 The lack of QBO-MJO connection in CMIP6 models *Geophys. Res. Lett.* **47** e2020GL087295

Kodera K, Mukougawa H and Fujii A 2013 Influence of the vertical and zonal propagation of stratospheric planetary waves on tropospheric blockings *J. Geophys. Res. Atmos.* **118** 8333–45

Kolstad E W, Breiteig T and Scaife A A 2010 The association between stratospheric weak polar vortex events and cold air outbreaks in the Northern Hemisphere *Q. J. R. Meteorol. Soc.* **136** 886–93

Kretschmer M, Cohen J, Matthias V, Runge J and Coumou D 2018 The different stratospheric influence on cold-extremes in Eurasia and North America *npj Clim. Atmos. Sci.* **1** 44

Labe Z, Peings Y and Magnusdottir G 2019 The effect of QBO phase on the atmospheric response to projected Arctic sea ice loss in early winter *Geophys. Res. Lett.* **46** 7663–71

Lawrence Z D, Perlwitz J, Butler A H, Manney G L, Newman P A, Lee S H and Nash E R 2020 The remarkably strong arctic stratospheric polar vortex of winter 2020: links to record-breaking arctic oscillation and ozone loss *J. Geophys. Res. Atmos.* **125** e2020JD033271

Lee S H, Furtado J C and Charlton-Perez A J 2019 Wintertime North American weather regimes and the arctic stratospheric polar vortex *Geophys. Res. Lett.* **46** 14892–900

Liang Z, Rao J, Guo D, Lu Q and Shi C 2022 Northern winter stratospheric polar vortex regimes and their possible influence on the extratropical troposphere *Clim. Dyn.* **59** 3741–61

Lorenz R, Stalhandske Z and Fischer E M 2019 Detection of a climate change signal in extreme heat, heat stress, and cold in Europe from observations *Geophys. Res. Lett.* **46** 8363–74

Lu H, Scaife A A, Marshall G J, Turner J and Gray L J 2017 Downward wave reflection as a mechanism for the stratosphere–troposphere response to the 11-Yr solar cycle *J. Clim.* **30** 2395–414

Lubis S W, Matthes K, Omrani N-E, Harnik N and Wahl S 2016 Influence of the Quasi-Biennial oscillation and sea surface temperature variability on downward wave coupling in the Northern Hemisphere *J. Atmos. Sci.* **73** 1943–65

Ma S and Zhu C 2019 Extreme cold wave over East Asia in January 2016: a possible response to the larger internal atmospheric variability induced by Arctic warming *J. Clim.* **32** 1203–16

Maycock A C and Hitchcock P 2015 Do split and displacement sudden stratospheric warmings have different annular mode signatures? *Geophys. Res. Lett.* **42** 10943–51

McIntyre M E 1982 How well do we understand the dynamics of stratospheric warmings? *J. Meteorol. Soc. Jpn.* II **60** 37–65

Messori G, Kretschmer M, Lee S H and Wendt V 2022 Stratospheric downward wave reflection events modulate North American weather regimes and cold spells *Weather Clim. Dyn.* **3** 1215–36

Millin O T, Furtado J C and Basara J B 2022 Characteristics, evolution, and formation of cold air outbreaks in the great plains of the United States *J. Clim.* **35** 4585–602

Perera A T D, Nik V M, Chen D, Scartezzini J-L and Hong T 2020 Quantifying the impacts of climate change and extreme climate events on energy systems *Nat. Energy* **5** 150–9

Perlwitz J and Harnik N 2003 Observational evidence of a stratospheric influence on the troposphere by planetary wave reflection *J. Clim.* **16** 3011–26

Plumb R A 1985 On the three-dimensional propagation of stationary waves *J. Atmos. Sci.* **42** 217–29

Pohlmann H, Müller W A, Kulkarni K, Kameswarrao M, Matei D, Vamborg F S E, Kadow C, Illing S and Marotzke J 2013 Improved forecast skill in the tropics in the new MiKlip decadal climate predictions *Geophys. Res. Lett.* **40** 5798–802

Randall D A, Tziperman E, Branson M D, Richter J H and Kang W 2023 The QBO–MJO connection: a possible role for the SST and ENSO *J. Clim.* **36** 6515–31

Rao J, Garfinkel C I, Ren R, Wu T and Lu Y 2023 Southern Hemisphere response to the Quasi-Biennial oscillation in the CMIP5/6 models *J. Clim.* **1** 1–45

Rao J, Garfinkel C I and White I P 2020 Impact of the Quasi-Biennial oscillation on the Northern Winter stratospheric polar vortex in CMIP5/6 models *J. Clim.* **33** 4787–813

Reichler T and Jucker M 2022 Stratospheric wave driving events as an alternative to sudden stratospheric warmings *Weather Clim. Dyn.* **3** 659–77

Richter J H, Anstey J A, Butchart N, Kawatani Y, Meehl G A, Osprey S and Simpson I R 2020 Progress in simulating the Quasi-Biennial oscillation in CMIP models *J. Geophys. Res. Atmos.* **125** e2019JD032362

Scaife A A *et al* 2014 Predictability of the quasi-biennial oscillation and its northern winter teleconnection on seasonal to decadal timescales *Geophys. Res. Lett.* **41** 1752–8

Scaife A A *et al* 2022 Long-range prediction and the stratosphere *Atmos. Chem. Phys.* **22** 2601–23

Shaw T A and Perlwitz J 2013 The life cycle of Northern Hemisphere downward wave coupling between the stratosphere and troposphere *J. Clim.* **26** 1745–63

Shaw T A, Perlwitz J and Weiner O 2014 Troposphere-stratosphere coupling: links to North Atlantic weather and climate, including their representation in CMIP5 models *J. Geophys. Res. Atmos.* **119** 5864–80

Shen X, Wang L, Scaife A A, Hardiman S C and Xu P 2022 The stratosphere-troposphere oscillation as the dominant intraseasonal coupling mode between the stratosphere and troposphere *J. Clim.* **36** 2259–76

Sigmond M, Scinocca J F, Kharin V V and Shepherd T G 2013 Enhanced seasonal forecast skill following stratospheric sudden warmings *Nat. Geosci.* **6** 98–102

Smith K L and Kushner P J 2012 Linear interference and the initiation of extratropical stratosphere-troposphere interactions *J. Geophys. Res. Atmos.* **117** D13107

Stockdale T N *et al* 2022 Prediction of the quasi-biennial oscillation with a multi-model ensemble of QBO-resolving models *Q. J. R. Meteorol. Soc.* **148** 1519–40

Sun L, Deser C and Tomas R A 2015 Mechanisms of stratospheric and tropospheric circulation response to projected Arctic sea ice loss *J. Clim.* **28** 7824–45

Thompson D W J, Baldwin M P and Wallace J M 2002 Stratospheric connection to Northern Hemisphere wintertime weather: implications for prediction *J. Clim.* **15** 1421–8

Vajda A, Tuomenvirta H, Juga I, Nurmi P, Jokinen P and Rauhala J 2014 Severe weather affecting European transport systems: the identification, classification and frequencies of events *Nat. Hazards* **72** 169–88

van Oldenborgh G J, Mitchell-Larson E, Vecchi G A, Vries H D, Vautard R and Otto F 2019 Cold waves are getting milder in the northern midlatitudes *Environ. Res. Lett.* **14** 114004

Wang L, Yang H, Wen Q, Liu Y and Wu G 2023 The Tibetan Plateau's far-reaching impacts on Arctic and Antarctic climate: seasonality and pathways *J. Clim.* **36** 1399–414

Woollings T, Charlton-Perez A, Ineson S, Marshall A G and Masato G 2010 Associations between stratospheric variability and tropospheric blocking *J. Geophys. Res.* **115** D06108

Wu Z and Reichler T 2020 Variations in the frequency of stratospheric sudden warmings in CMIP5 and CMIP6 and possible causes *J. Clim.* **33** 10305–20

Xiang B, Lin S, Zhao M, Johnson N C, Yang X and Jiang X 2019 Subseasonal week 3–5 surface air temperature prediction during boreal wintertime in a GFDL model *Geophys. Res. Lett.* **46** 416–25

Yu Y, Cai M, Ren R and van den Dool H M 2015 Relationship between warm airmass transport into the upper polar atmosphere and cold air outbreaks in winter *J. Atmos. Sci.* **72** 349–68

Zhang J, Xie F, Ma Z, Zhang C, Xu M, Wang T and Zhang R 2019 Seasonal evolution of the Quasi-biennial oscillation impact on the Northern Hemisphere polar vortex in winter *J. Geophys. Res. Atmos.* **124** 12568–86

Zhang P, Wu Y, Simpson I R, Smith K L, Zhang X, De B and Callaghan P 2018 A stratospheric pathway linking a colder Siberia to Barents-Kara Sea sea ice loss *Sci. Adv.* **4** eaat6025

Zhang R, Screen J A and Zhang R 2022 Arctic and Pacific Ocean conditions were favorable for cold extremes over Eurasia and North America during winter 2020/21 *Bull. Am. Meteorol. Soc.* **103** E2285–301

Zou C and Zhang R 2024 Arctic sea ice loss modulates the surface impact of autumn stratospheric polar vortex stretching events *Geophys. Res. Lett.* **51** e2023GL107221

Zou C, Zhang R, Zhang P, Wang L and Zhang R 2023 Contrasting physical mechanisms linking stratospheric polar vortex stretching events to cold Eurasia between autumn and late winter *Clim. Dyn.* **62** 2399–417

Zuo J, Xie F, Yang L, Sun C, Wang L and Zhang R 2022 Modulation by the QBO of the relationship between the NAO and Northeast China temperature in late winter *J. Clim.* **35** 4395–411